INVESTIGATION OF DIFFERENT FAN NOISE PREDICTION METHODS

Clemens JUNGER, Manfred KALTENBACHER

TU Wien, Institute of Mechanics and Mechatronics, Getreidemarkt 9, 1060 Vienna, Austria

SUMMARY

Different fan noise prediction methods were compared with experimental data. For this purpose measurement data was used from a rotor benchmark of a low speed axial fan as reference. For computing the sound pressure level, the methods according to VDI 2081, VDI 3731 and Sharland have been applied. For spectral data, the method of Költzsch and a hybrid aeroacoustic method based on incompressible flow simulations coupled with an acoustic propagation simulation were used.

INTRODUCTION

Noise prediction is a necessary stage in all modern fan design processes. The different existing methods can be categorized in three different classes according to [1]. The first class contains empirical methods, based on geometry and operating conditions. They are very fast and easy to apply. The second class contains semi-empirical methods that are partly based on flow quantities from measurements or simulations. These methods shall represent the actual operating conditions in a better way, but are more time consuming since the flow quantities must be obtained. The third class contains methods that compute the noise radiation directly from fluctuating quantities of the transient flow. These methods give a good insight in the contribution to the overall sound level from different sound sources. Due to the need of transient flow data, this class of methods is highly demanding towards computational power. A fourth category for the direct aeroacoustic computation was suggested later on [2]. In our contribution we compare different methods from class one to three and apply them to a low-pressure axial fan. The fan used for the application is a previously published benchmark case [3]. This fan was already investigated numerically in [4].

THE INVESTIGATED FAN

The generic fan is designed to be a typical fan used in commercial applications in terms of size and operating conditions. The rotor benchmark fan provides an extensive amount of measurement data

including aerodynamic performance (volume flow rate, pressure rise and efficiency), wall pressure fluctuations in the tip gap region, fluid mechanical quantities on the fan suction and pressure side (velocity in three spatial direction and turbulent kinetic energy) and acoustic spectra at different microphone positions. The fan was designed with NACA 4510 profile blades and zero blade skew for easy reproducibility. The design parameters are shown in Tab. 1.

Table 1: Fan characteristics

fan diameter	495 mm
hub diameter	248 mm
tip clearance	2.5 mm
blades	9
volumetric flow	$1.4\,\mathrm{m}^3/\mathrm{s}$
total-to-static pressure difference	150 Pa
rotational speed	1486 1/min
chord length hub	103 mm
chord length tip	58 mm
Reynolds number hub	$1.25 \cdot 10^5$
Reynolds number tip	$1.5 \cdot 10^5$

The fan geometry and the measurement results can be obtained online (`https://eaa-bench.mec.tuwien.ac.at/benchmarks/acoustics_involving_heterogeneous_and_moving_fluids/axial_fan`). The measurements were made in an anechoic inlet test chamber. The measured sound power level at the design point of the fan was measured over 30 s and was computed from 100 Hz to 10 kHz as $L_\mathrm{W} = 87.3$ dB and will be used as the reference for the sound prediction methods compared later on.

CLASS 1 METHODS

VDI 2081

The VDI 2081 standard [5] provides a relation for the outlet duct sound power level L_W in the form of

$$L_\mathrm{W} = L_{\mathrm{W}S} + 10 \lg \dot{V} + 5(\gamma - 1) \lg \Delta p_\mathrm{t} \quad \text{in dB}\,, \tag{1}$$

which is simply a function of the volume flow rate $\dot{V}$, the total pressure increase Δp_t between the inlet chamber and the ambience, the specific sound power level $L_{\mathrm{W}S}$ and the Mach number exponent γ. For axial fans the Mach number exponent can be assumed to $\gamma = 5$ and $L_{\mathrm{W}S} = 42$ dB and the formula becomes

$$L_\mathrm{W} = L_{\mathrm{W}S} + 10 \lg \dot{V} + 20 \lg \Delta p_\mathrm{t} \quad \text{in dB}\,, \tag{2}$$

which is very similar to the estimation of Madison [6]. This method gives a simple estimation of the overall sound power level, but it does not take any geometric properties into account.

VDI 3731

The VDI 3731 standard [7] is based on Regenscheit [8], where the sound power level is assumed to be proportional to the aerodynamic power loss and an exponent of the circumferential Mach number

$$P \propto \dot{V}\Delta p_t \left(\frac{1}{\eta_i} - 1\right) (Ma_u)^m \,, \tag{3}$$

with the inner efficiency η_i (efficiency without losses due to leakage and friction in bearings), the Mach number exponent m and the circumferential Mach-number Ma_u. The circumferential Mach-number is

$$Ma_u = \frac{u_a}{c_0} = \frac{\pi D n}{c_0} \,, \tag{4}$$

with the diameter D, the rotational speed n and the speed of sound c_0 In a logarithmic form this leads to

$$L_W = L_{WS} + 10\,\mathrm{lg}\left[\frac{\dot{V}}{\dot{V}_0}\frac{\Delta p_t}{\Delta p_0}\left(\frac{1}{\eta} - 1\right)\right] + 10\,m\,\mathrm{lg}\,[Ma_u] \quad \text{in dB}\,, \tag{5}$$

with the reference values $\dot{V}_0 = 1\,\mathrm{m}^3/\mathrm{s}$ and $\Delta p_0 = 1\,\mathrm{Pa}$. Because the measurement of the inner efficiency η_i is difficult, it is replaced with the total-to-static efficiency of the fan η. For axial fans, the specific sound power level can be assumed to be $L_{WS} = 96.6\,\mathrm{dB}$ and the exponent to $m = 3.16$. The total-to-static efficiency of the fan is

$$\eta = \frac{\dot{V}\Delta p_t}{2\pi n M} \,, \tag{6}$$

with M the measurement torque and n the rotational velocity.

CLASS 2 METHODS

This class contains a wide range of methods, like Amiet's theory [9] that is designed for airfoil noise and can also be adapted to rotating airfoils. Furthermore, the TNO type models should be mentioned [10], [11] that are used to compute trailing edge noise. But for the compactness of this contribution, just the method of Sharland [12] and Költzsch [13] will be addressed.

Sharland

The method of Sharland [12] assumes the blades to be flat plates that are radiating incoherently and without any interfering effects. The radiated sound power is split in contributions from three different effects. The first one is from the turbulent inflow (ti), the second one from pressure fluctuation in the boundary layer (tbl) and the third from vortex shedding (vs)

$$P \;= P_{\text{ti}} + P_{\text{tbl}} + P_{\text{vs}} \,. \tag{7}$$

Each term is approximated with an integral over the blade from the inner radius r_i to the outer radius r_o.

$$P_{\text{ti}} \approx z\frac{1}{48\pi}\frac{\rho}{c_0^3}\int_{r_i}^{r_o} l\Phi^2 w_\infty^6 Tu^2 \mathrm{dr} \tag{8}$$

$$P_{\text{tbl}} \approx z\cdot 10^{-7}\frac{\rho}{c_0^3}\int_{r_i}^{r_o} l w_\infty^6 \mathrm{dr} \tag{9}$$

$$P_{\text{vs}} \approx z\frac{1}{120\pi}\frac{\rho}{c_0^3}\int_{r_i}^{r_o} l w_\infty^6 Re^{-0.4} \mathrm{dr} \tag{10}$$

The noise from the turbulent inflow depends on turbulent intensity Tu, the relative velocity w_∞, the chord length l and the gradient of lift coefficient Φ, which was approximated by Sharland as $\Phi \approx 0.9\pi$. The integrals may be approximated by an evaluation of the quantities at a representative radius of the blade. A height of about 70% of the blade seem to be often applicable [14]. For highly skewed fans this might be different. Each noise mechanism is multiplied by the number of blades z. The vortex shedding noise might be neglected for airfoils with sharp trailing edge. A drawback of the method of Sharland is that it does not provide any spectral information.

Költzsch

In contrast to the Sharland method, the Költzsch method [13] provides spectral information. In this method the power spectral density (PSD) is described as a combination of the turbulent inflow and turbulent boundary layer

$$S = S_{\text{ti}} + S_{\text{tbl}}\,. \tag{11}$$

The PSD of the turbulent inflow is approximated with the spectral energy density S_w of the inflow and the dimensions of the blade l and b

$$S_{\text{ti}}(f) \approx z \cdot \frac{0.81\pi}{48}\frac{\rho}{c_0^3} \cdot w_\infty^4 \cdot S_w(f) \cdot l \cdot b\,. \tag{12}$$

The spectral energy density is computed as

$$S_w(f) = \bar{U} \cdot Tu^2 \cdot \Lambda \cdot 10^{F(f)/10}\,, \tag{13}$$

with the flow mean inflow velocity $\bar{U}$, the turbulent intensity, a turbulent length scale Λ and a regression polynomial

$$F(f) \approx \sum_{k=1}^{4} a_k \left(\lg\left(\frac{f\Lambda}{c}\right)\right)^{k-1}\,, \tag{14}$$

where the coefficients for the polynomial are

$$a_k = -9.784; -19.001; -5.548; -0.060\,. \tag{15}$$

The PSD of the turbulent boundary layer for a fan in a sound hard duct computes as

$$S_{\text{tbl}} = z\frac{\pi}{4}\frac{f}{\rho c_0^2 r_o(1-\nu^2)^2} S_{\text{bl}}(f)\psi\,, \tag{16}$$

with the PSD of the lift forces S_{bl}, a radiation function ψ that can be approximated as $\psi \approx 1$ for low Mach-number flows and the relation of the outer diameter to the hub ν. The approximation of the PSD of the lift forces S_{bl} is described by three different functions, depending on the frequency

$$S_{\text{bl}}(f) \approx \begin{cases} \frac{bl^2 w_\infty}{5\pi f} S_p(f) & \text{for} \quad \frac{\pi f l}{w_\infty} \leq 2 \\ \frac{2blw_\infty^2}{5\pi^2 f^2} S_p(f) & \text{for} \quad 2 < \frac{\pi f l}{w_\infty} \leq \frac{15}{\pi} \\ \frac{6bw_\infty^3}{\pi^4 f^3} S_p(f) & \text{for} \quad \frac{15}{\pi} \leq \frac{\pi f l}{w_\infty} \end{cases}\,. \tag{17}$$

The PSD of the wall is computed with the approximated boundary layer displacement thickness δ^* and an approximation formula $G(St_{\delta^*})$

$$S_p(f) = \rho^2 w_\infty^3 \delta^* G(St_{\delta^*})\,. \tag{18}$$

The approximated boundary layer displacement thickness can be estimated with the known relation for a flat plate

$$\frac{\delta^*}{l} = 0.05 Re_l^{-0.2} \tag{19}$$

and the approximation formula is

$$G(St_{\delta^*}) = \frac{0.01}{1 + 4.1985St_{\delta^*} + 0.454St_{\delta^*}^6} \,. \tag{20}$$

The vortex shedding noise from the trailing edge is neglected in this estimation.

CLASS 3 METHOD

Since a direct simulation of the radiated sound is too expensive, a hybrid aeroacoustic method is used. Our numerical approach from the third class is based on a forward coupling between a flow simulation with ANSYS Fluent and an aeroacoustic source term and wave propagation computation with multiphysics research software CFS++ [15].

Flow Simulation

To obtain the transient flow field we use an incompressible flow simulation in ANSYS Fluent with approximately 48 M cells on an unstructured mesh. A schematic of the computational domain is shown in Fig. 1. To simulate the rotation of the fan, a rotating mesh region is used in the duct. The inlet

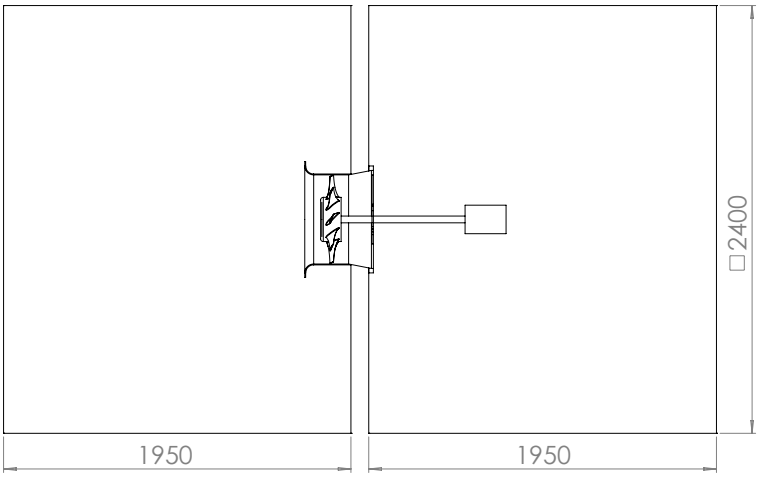

Figure 1: computational domain for the flow simulation

chamber (on the left side) and the outlet area (on the right side) were modeled as stationary domains. The three domains were connected with nonmatching interfaces. The boundary layers are resolved to guarantee the $y^+ < 1$ condition. A map of y^+ on the fan surface is shown in Fig. 2 (left). On the right side of Fig. 2 the vortex structure is displayed by the Q-criterion.

The inlet is modeled as a mass-flow-inlet and the outlet as a pressure outlet with zero pressure. As a turbulence model the stress blended eddy simulation (SBES) [16] was used. To reduce the computational effort, the geometry of the engine and shaft were reduced to a single block with the same dimensions. To account for CFL ≤ 1 a time step size of $\Delta t = 1 \cdot 10^{-7}$ s has to be used. For the transient results an export time of 0.13 s was used, which corresponds to 3.2 revolutions. As just recently noticed by the authors Fluent is not recommended for rotor simulations with interfaces, so the validity of the simulation needs further investigation.

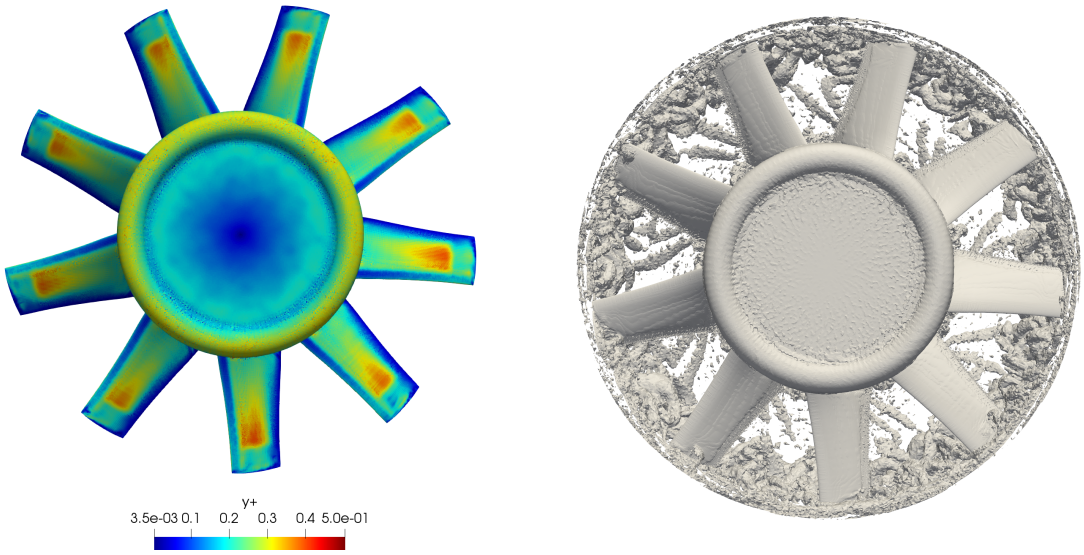

Figure 2: Simulation conditions. y^+ criterion (left) and vortex structure by the Q-criterion (right).

Acoustic Simulation

The aeroacoustic analogy for the used hybrid acoustic method is the perturbed convective wave equation (PCWE) as described in [17]. This analogy was already used successfully in [18] and [19]. In this analogy the wave equation describing the acoustic propagation is:

$$\frac{1}{c_0^2}\frac{D^2\varphi^a}{Dt^2} - \nabla\cdot\nabla\varphi^a = -\frac{1}{\rho_0 c_0^2}\frac{Dp^{ic}}{Dt}\,, \tag{21}$$

with the acoustic potential φ^a, constant speed of sound c_0 and density ρ_0 and the incompressible pressure p^{ic} from the flow simulation. The acoustic source term on the right hand side is computed with the substantial derivative of the incompressible pressure:

$$\frac{\mathrm{D}p^{\mathrm{ic}}}{\mathrm{D}t} = \left(\frac{\partial}{\partial t} + (\bar{\mathbf{u}} - \mathbf{u}_{\mathrm{r}})\cdot\nabla\right) p^{\mathrm{ic}}\,, \tag{22}$$

where the mean velocity $\bar{\mathbf{u}}$ has to be corrected with the grid velocity $\mathbf{u}_{\mathrm{r}}$ in the rotating region. Thereby, (21) is solved with the finite element method on a discretized domain. To obtain the acoustic pressure p^a from this solution, the substantial derivative has to be applied to the velocity potential

$$p^a = \rho_0 \frac{\mathrm{D}}{\mathrm{D}t}\varphi^a\,. \tag{23}$$

In the discretized domain, different boundary conditions can be applied to account for reflections or absorption, which is difficult to realize with integral solutions.

The acoustic computation domain is identical to the domain of the flow simulation, except for the size of the inlet and outlet chamber. These two domains are surrounded by a perfectly matched layer, to account for the anechoic conditions. All other walls are modeled sound hard. The acoustic mesh is generated with a maximum spacing of $23.5\,\mathrm{mm}$ to resolve frequencies up to $1500\,\mathrm{Hz}$ with at least ten linear elements; the number of mesh nodes results in approximately $2.3\,\mathrm{M}$. The rotating domain is again connected with nomatching interfaces to the other domains. The time step size for the acoustic simulation is $\Delta t = 2\cdot 10^{-5}\,\mathrm{s}$.

RESULTS

The over all sound power level of the two class 1 methods and the Sharland method are displayed in Tab. 2. Compared to the measurement, the Sharland method has the smallest difference, but the class 1 methods are very close as well.

Table 2: predicted sound power level

	L_w dB	$\Delta L_{w,A}$ dB
Measurement	87.3	–
VDI 2081	85.6	1.7
VDI 3731	88.7	1.4
Sharland	86.4	0.9

The power spectral density (PSD) of the measurement, the Költzsch method and the simulation result of the class 3 method are shown in Fig. 3. The black line is the measurement signal with a measurement time of 30.0 s and the gray lines are sections of the measurement signal with the same length in time as the simulation signal of 0.13 s. The green line is the result of the Költzsch method. In the low

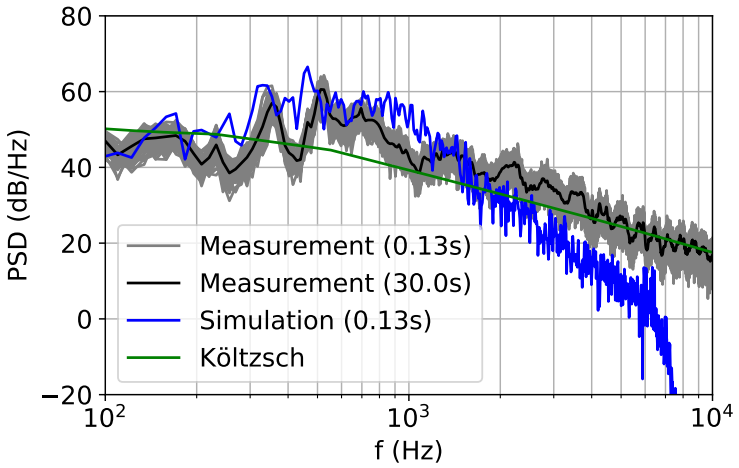

Figure 3: Comparison of power spectral density from measurement, simulation and Költzsch method

frequency range, the PSD is predicted to be slowly falling with a steeper slope above 1 kHz. The overall behavior is met, but no tonal components can be obtained with this method. The blue line is the result of the class 3 method. It overestimates the PSD at low frequency, but represents the tonal components of the signal. In the higher frequency range the PSD is underestimated. Above 6 kHz the grid resolution is too coarse to resolve the acoustic waves.

CONCLUSION

In this setup, the prediction methods of class 1 show good agreement for the overall sound pressure level. They are very easy to apply and need just rough information about the fan and its operating conditions, but it can not be assumed that this good agreement can be transferred blindly to other geometries. Especially since this is a rather basic fan design without any geometry optimization. The

class 2 methods need at least some information about the flow conditions that have to be gathered empirically. The Sharland method predicts the overall sound power level even better. Due to the separate description of the sound sources it can be stated that the main contribution is from the turbulent inflow. The Költzsch method gives a good behavior of the frequency distributed power spectral density. Unfortunately, none of these methods can predict the tonal components of the fan. In contrast to that, the used class 3 method can represent the tonal components but is highly expensive in computational effort.

REFERENCES

[1] T. Caroulus. *Noise Proves Nothing - Sources of Fan Noise and Their Prediction (Keynote lecture)*. In *Fan2012*, Senlis, France, **2012**.

[2] S. Moreau. *Numerical and analytical predictions of low-speed fan aeroacoustics (Keynote lecture)*. In *Fan2015*, Lyon, France, **2015**.

[3] F. Zenger, C. Junger, M. Kaltenbacher, and S. Becker. *A benchmark case for aerodynamics and aeroacoustics of a low pressure axial fan*. SAE Technical Papers, (2016-01-1805), **2016**.

[4] C. Junger, F. Zenger, A. Reppenhagen, M. Kaltenbacher, and S. Becker. *Numerical simulation of a benchmark case for aerodynamics and aeroacoustics of a low pressure axial fan*. In *Proceedings 45th International Congress and Exposition of Noise Control Engineering, inter.noise*, pages 741–747, Hamburg, Germany, **2016**.

[5] VDI 2081. *Noise generation and noise reduction in air-conditioning systems*, **2001**.

[6] R. D. Madison. *Fan Engineering (Handbook)*. Buffalo Forge Company, Buffalo N.Y., **1949**.

[7] VDI 3731 Blatt 2. *Emissionskennwerte technischer Schallquellen – Ventilatoren*, **1990**.

[8] B. Eck. *Ventilatoren*. Springer-Verlag, Berlin-Heidelberg, **1991**.

[9] R. K. Amiet. *Noise due to turbulent flow past a trailing edge*. J. Sound Vib., 47(3):387–393, **1976**.

[10] W. K. Blake. *Mechanics of Flow-Induced Sound and Vibration*, volume I and II of *Applied Mathematics and Mechanics*. Academic Press, **1986**.

[11] R. Parchen. *Progress report DRAW: A prediction scheme for trailing edge noise based on detailed boundary layer characteristics*. TNO Institute of Applied Physics, **1998**.

[12] Sharland, I. J. *Sources of Noise in Axial Flow Fans*. J. Sound Vib., 1(3):302–322, **1964**.

[13] P. Költzsch. *Ein Beitrag zur Berechnung des Wirbellärms von Axialventilatoren*. In *Jahrestagung der Deutschen Akustischen Gesellschaft*, Frankfurt am Main, Germany, **1993**.

[14] T. Carolus. *Ventilatoren*. Vieweg+Teubner Verlag, Springer Fachmedien Wiesbaden, **2013**.

[15] M. Kaltenbacher. *Numerical Simulation of Mechatronic Sensors and Actuators*. Springer, Berlin, 3. edition, **2015**.

[16] F. R. Menter. *Stress-Blended Eddy Simulation (SBES) - A new Paradigm in hybrid RANS - LES Modeling (Keynote lecture)*. In *Sixth HRLM Symposium*, Strasbourg University, France, **2016**.

[17] M. Kaltenbacher, A. Hüppe, A. Reppenhagen, F. Zenger, and S. Becker. *Computational aeroacoustics for rotating systems*. In *22nd AIAA/CEAS Aeroacoustics Conference*, Lyon, France, **2016**.

[18] A. Hüppe, M. Kaltenbacher, A. Reppenhagen, F. Zenger, S. Becker, and K. Habr. *Computational Aeroacoustics for Ducted Fans*. In *The 22nd International Congress on Sound and Vibration*, Florence, Italy, **2015**.

[19] M. Kaltenbacher, A. Hüppe, A. Reppenhagen, F. Zenger, and Becker S. *Computational Aeroacoustics for Rotating Systems with Application to an Axial Fan*. AIAA J., 55(11):3831–3838, **2017**.

ACKNOWLEDGEMENTS

The authors gratefully acknowledge the support by ANSYS, Inc. The computational results presented have been achieved using the Vienna Scientific Cluster (VSC).